RSC Advances

PAPER

View Article Online
View Journal | View Issue

Cite this: *RSC Adv.*, 2020, **10**, 29187

Sulfonated SnO_2 nanocatalysts *via* a self-propagating combustion method for esterification of palm fatty acid distillate

N. Nabihah-Fauzi,[ab] N. Asikin-Mijan,[c] Mohd Lokman Ibrahim,[b] Hasdiyana Hashim,[b] Suzana Yusup,[d] Y. H. Taufiq-Yap[ef] and Mohd Sufri Mastuli *[ab]

Received 9th June 2020
Accepted 17th July 2020

DOI: 10.1039/d0ra05110a

rsc.li/rsc-advances

Biodiesel derived from palm fatty acid distillate (PFAD) was produced *via* catalytic esterification using sulfonated tin oxide (HSO_3^-/SnO_2) as the superacid solid catalyst. In this work, the SnO_2 catalyst was synthesised by the self-propagating combustion (SPC) method, and activated using chlorosulfonic acid. The SPC method was able to produce nano-sized particles with homogenous size and shape that were anchored with many HSO_3^- ions, resulting in more exceptional acid properties that effectively esterified the PFAD feedstock into FAMEs (fatty acid methyl esters). Several studies based on metal oxide-based catalysts were also included for comparison. Under the optimised conditions of 9 : 1 (methanol-to-PFAD molar ratio), 4 wt% (catalyst loading), 100 °C (reaction temperature) and 3 h (reaction time), the FFA conversion and FAME yield were 98.9% and 93.8%, respectively. Besides, the sulfonated SnO_2-spc catalyst can be reused in up to five consecutive cycles with an acceptable esterification performance and minimal sulfur leaching. It is worth mentioning that the SPC method is a greener and simpler technique to obtain the nanocatalysts. Overall, the production of FAME from low value, cheaper, abundant, and non-edible PFAD feedstock, assisted by a non-transition metal oxide of sulfonated SnO_2 catalyst, could reduce the cost of biodiesel production.

1. Introduction

The depletion of fossil fuels and their increasing demand, as well as environmental concerns, have triggered global awareness to enforce the utilisation of renewable fuels such as biodiesel.[1] Biodiesel is a mixture of fatty acid methyl esters (FAMEs),[2] which can be obtained *via* transesterification of triglycerides (TGs) or esterification of free fatty acids (FFAs), that react with a short-chain alcohol (methanol) in the presence of a catalyst.[3] Biodiesel offers several advantages over fossil fuels, such as being non-toxic, biodegradable and environmentally benign, with almost zero emission of sulfur dioxide (SO_x), aromatic compounds and other pollutants.[4] Indeed, there is a small net contribution of carbon dioxide (CO_2) when the whole life-cycle is considered. In Malaysia, B5 biodiesel consisting of a blend of 5% palm oil-derived biodiesel and 95% conventional diesel has been introduced for the industrial market. Recently, B20 biodiesel was launched by the Malaysian government and will be implemented in the year 2021. However, the possibility to increase the percentage up to 100% pure biodiesel (B100) is a hard vision to achieve because edible palm oil is not only costly but has to compete with the food industry. Thus, the utilisation of non-edible oils, waste oils or waste fats could reduce biodiesel production costs by 60–90%.[5] The usage of these feedstocks would avoid the controversy of the "food *versus* fuel debate" dilemma.

As the world's largest crude palm oil (CPO) exporter and the second-largest CPO producer, Malaysia produces many by-products from the refinery process of CPO, and one of them is called palm fatty acid distillate (PFAD). PFAD contains more than 80% FFAs with palmitic and oleic acids as the main components. The remaining 5–15% are triglycerides, partial glycerides and unsaponifiable components such as vitamin E, sterols, squalene, and volatile compounds.[6] The amount of FFA can be varied depending on the fat degradation in the fruit by enzymes after harvesting.[7] Many studies have been reported on the esterification of PFAD into biodiesel, which is assisted by acid catalysts.

[a]*School of Chemistry and Environment, Faculty of Applied Sciences, Universiti Teknologi MARA, 40450 Shah Alam, Selangor, Malaysia*

[b]*Centre for Functional Materials and Nanotechnology, Institute of Science, Universiti Teknologi MARA, 40450 Shah Alam, Selangor, Malaysia. E-mail: mohdsufri@uitm.edu.my; Fax: +603 5543 4562; Tel: +603 5544 3096*

[c]*Department of Chemical Sciences, Faculty of Science and Technology, Universiti Kebangsaan Malaysia, 43600 UKM Bangi, Selangor, Malaysia*

[d]*Chemical Engineering Department, HiCoE, Biomass Processing Cluster, Centre for Biofuel and Biochemical Research, Institute of Sustainable Building, Universiti Teknologi PETRONAS, 32610 Seri Iskandar, Perak, Malaysia*

[e]*Catalysis Science and Technology Research Centre, Faculty of Science, Universiti Putra Malaysia, 43400 UPM Serdang, Selangor, Malaysia*

[f]*Chancellery Office, Universiti Malaysia Sabah, 88400 Kota Kinabalu, Sabah, Malaysia*

Heterogeneous-catalysed esterification using metal oxide-based catalysts is widely used for the esterification of FFAs.[8] These catalysts are active for biodiesel synthesis up to 80% under specific conditions. Metal oxides are known to possess Lewis–Brønsted acid sites,[9] which are stable in air and heat,[10] and ease of catalyst synthesis. Among the reported metal oxides, tin oxide (SnO_2) shows a remarkable catalytic performance in both TG transesterification and FFA esterification. However, SnO_2 alone is not effective due to the lack of acid active sites. To overcome this issue, the SnO_2 catalyst should be treated with a strong acid such as sulfuric acid[11] or doped with other metal oxides such as silica (SiO_2),[12] cobalt oxide (Co_2O_3)[13] or alumina (Al_2O_3).[14] However, in this study, sulfonation treatment has been selected to improve the SnO_2 acidity. According to Fadhil and his co-workers, acid treatment is an important approach to modify the hydrophilicity on the catalyst surface. Surface hydrophilicity plays a crucial part during esterification as it serves as the anchoring site of polar substrates between FFA and methanol.[15] During the post-sulfonation treatment, sulfonic acid groups ($-SO_3H$) bond covalently on the catalyst surface, highly increasing the acid strength as active sites and improving the stability of the catalyst.[16]

Various methods such as precipitation,[2] sol–gel,[11] solid-state[17] and thermal decomposition[18] have been used to synthesise SnO_2 catalysts. Some of these methods have encountered problems such as the formation of undesirable phases, the requirement of complicated equipment or being time-consuming due to multiple steps. Therefore, a facile synthesis method known as self-propagating combustion (SPC) is employed to synthesise the SnO_2 catalyst. The SPC method is an exothermic redox reaction between a metal nitrate and an appropriate fuel (oxidising agent) to produce the nanocrystalline metal oxide.[19] Evinced by Xue and his co-workers,[20] the SPC method offers many advantages such as energy-saving, short reaction time and straightforward setup that produces a high yield product with good chemical homogeneity[21] and high purity.[22]

Even though sulfonated SnO_2 is a promising catalyst for biodiesel production, the esterification performance is still far from ideal because of the incapability of the sulfonated anion to be fully anchored on the SnO_2 catalyst surface. Thus, this work aims to overcome this problem. A sulfonated SnO_2 catalyst was synthesised *via* the SPC method, and the physicochemical properties were investigated. The catalytic performance of the esterification of the PFAD feedstock to produce biodiesel was evaluated. The influencing factors, such as methanol-to-PFAD molar ratio, catalyst loading, reaction temperature and reaction time, were also investigated and optimised. Finally, the catalyst reusability and leaching analysis under the optimised reaction conditions were studied.

2. Experimental section

2.1 Chemicals

Tin chloride dihydrate ($SnCl_2 \cdot 2H_2O$; 98% purity) and commercial tin oxide (SnO_2; 99% purity) were purchased from Sigma-Aldrich Co., St. Louis, MO, USA. Citric acid monohydrate ($C_6H_8O_7 \cdot H_2O$; 99.5% purity) and potassium hydroxide (KOH; 85% purity) were obtained from Friendemann Schmidt, Washington, USA. Concentrated chlorosulfonic acid (HSO_3Cl; 99% purity) and hydrochloric acid (HCl; 37% purity) were supplied by R&M Chemicals. Other analytical grade solvents such as methanol (CH_3OH; 99.9% purity), ethanol (C_2H_5OH; 99.9% purity), *n*-hexane (C_6H_{14}; 98% purity), isopropanol (C_3H_8O; 99.8% purity), toluene (C_7H_8; 99.5% purity), and acetone (C_3H_6O; 99.5% purity) were provided by Merck KGaA, Darmstadt, Germany. All the chemicals were used as received without any purification. The reference standards of FAME (methyl oleate, methyl linoleate, methyl palmitate, methyl myristate and methyl stearate) and internal standard (methyl heptadecanoate) with 99.9% purity were purchased from Fluka Analytical, USA. The PFAD feedstock was supplied by Jomalina R&D, Sime Darby Sdn. Bhd., Klang, Selangor, Malaysia and the feedstock properties were analysed according to the American Oil Chemists' Society (AOCS) guidelines, including moisture content (AOCS Ca 2b-38), saponification value (AOCS TI 1a-64) and acid value (AOCS Cd 3d-63).

2.2 Catalyst synthesis

The SnO_2 was synthesised *via* the SPC method, as reported previously.[23] The formed catalyst was labelled as SnO_2-spc. About 3 g of $SnCl_2 \cdot 2H_2O$ and 0.28 g of $C_6H_8O_7 \cdot H_2O$ were dissolved in 5 ml of deionised water. Both aqueous mixtures were vigorously stirred to form a homogenous solution. Then, it was heated at 350 °C without stirring until the combustion reaction occurred, and a blackish-grey powder was formed. The dried precursor powder was calcined at 600 °C for 6 h to give a pure SnO_2-spc catalyst. For comparison, the commercial SnO_2, which was labelled as SnO_2-com, was also used as a catalyst.

Afterwards, the SnO_2-com and SnO_2-spc catalysts were sulfonated using concentrated HSO_3Cl. Approximately 2 ml of HSO_3Cl was slowly added into 2 g of each catalyst and stirred under N_2 flow for 1 h at ambient temperature. Next, both sulfonated catalysts were rinsed with methanol to remove the Cl^- ions as well as the unattached HSO_3^- ions from the catalyst surface. The excess solvent was also separated through centrifugation, and the sulfonated solid catalysts were dried in an oven at 100 °C overnight.

2.3 Catalyst characterisation

All the catalysts (SnO_2-com, SnO_2-spc, sulfonated SnO_2-com and sulfonated SnO_2-spc) were characterised using various instruments. The thermal decomposition of the precursor obtained from the SPC method was analysed using a simultaneous thermogravimetric analyser (STA; SETARAM SETSYS Evolution 1750). This instrument gave the thermogravimetric analysis (TGA) and differential scanning calorimetry (DSC) graphs simultaneously. The TGA/DSC measurements were done in an air atmosphere at a heating rate of 10 °C min^{-1}. Powder X-ray diffraction (PANanalytical X'Pert Pro MPD) was used to study the phase and structure of the catalysts. The XRD equipped with a solid-state detector was operated at 45 kV and 40 mA with a Ni-filter and Cu-Kα radiation ($\lambda = 1.541$ Å). All of the catalysts were

scanned at 2θ from 20° to 80° with a scanning rate of 2° min^{-1} and a scanning step of 0.02°. A Bragg–Brentano optical configuration in ambient conditions was used for data collection. The sample was also analysed in spinning mode to reduce the effects of preferred orientation. The surface morphology, elemental composition and elemental mapping of the catalysts were investigated using field emission scanning electron microscopy that was integrated with an energy dispersive X-ray (FESEM-EDX; JEOL JSM-7600 F). All the samples were coated on conductive carbon paint for the FESEM-EDX analyses. The working distance and accelerating voltage were 6 mm and 3 kV for the FESEM morphology, and were 15 mm and 20 kV for the elemental composition. The EDX detector is an Oxford INCA X-MAC 51 XMX 0021. The amount of sulfur on the catalyst surface was also analysed using a CHNS elemental analyser (Thermo Scientific Flash 2000 elemental analyser). The N_2 adsorption–desorption isotherms of the catalysts were measured at −196 °C by a BELSORP-mini II instrument from BEL Japan Inc. Before the measurement, the sample was degassed at 200 °C for 6 h in a vacuum oven. The isotherm was further analysed using the Brunauer–Emmett–Teller (BET) method to give the specific surface area, total pore volume and average pore diameter of the catalysts. The acidity properties of the catalysts were studied using temperature-programmed desorption of ammonia (TPD-NH_3; Thermo Finnigan TPDRO 1100) equipped with a thermal conductivity detector (TCD). About 50 mg of each catalyst was pre-treated with N_2 flow for 30 min at 250 °C, followed by exposure to NH_3 gas for 1 h at ambient temperature to allow the adsorption of NH_3 onto the catalyst surface. The excess NH_3 was subsequently flushed with N_2 flow at a rate of 20 ml min^{-1} for 30 min. The desorption of NH_3 from the acid sites of the catalyst was detected by a thermal conductivity detector under helium gas flow (30 ml min^{-1}) from 50 to 900 °C and was held for 30 min.

2.4 Catalytic esterification of the PFAD feedstock

The esterification of the PFAD feedstock with methanol was performed in a 250 ml two-necked round-bottom flask equipped with a reflux condenser, oil bath, magnetic stirrer and thermometer. For catalyst screening, about 5 g of PFAD was mixed with 3 wt% of the studied catalyst and 5.5 ml of methanol (methanol-to-PFAD molar ratio of 9 : 1). The mixture was refluxed at 100 °C for 3 h under continuous stirring. After the reaction completed, the resultant product was cooled down to room temperature before being centrifuged to separate the solid acid catalyst from the mixture of methanol and biodiesel. Then, the mixture was left overnight for complete separation between methanol and biodiesel without solidification. The obtained biodiesel was heated at 70 °C until the methanol layer evaporated. Meanwhile, for optimization, the classical OVAT (one variable at time) technique was employed by varying the methanol–PFAD molar ratio (3 : 1, 6 : 1, 9 : 1, 12 : 1, 15 : 1), catalyst loading (1, 2, 3, 4, 5 wt%), reaction temperature (80, 100, 120, 140, 160 °C) and reaction time (1, 2, 3, 4, 5 h). All of the esterification products were further treated similarly as above, followed by acid value (AV) determination using the titration method (AOCS Cd 3d-63). The acid value of the PFAD feedstock and PFAD biodiesel are important to calculate the FFA content in each product, in which the FFA conversion depicts the catalyst performance in the esterification reaction. The AV and FFA conversion were calculated according to eqn (1) & eqn (2).

$$\mathrm{AV} = \frac{A \times N \times\ 56.11}{w} \quad (1)$$

A represents the volume (ml) of KOH, N refers to the normality of KOH, 56.11 g mol^{-1} is the molar mass of KOH and w is the mass (g) of the sample.

$$\text{FFA conversion } (\%) = \frac{\mathrm{AV_f} - \mathrm{AV_p}}{\mathrm{AV_f}} \times 100 \quad (2)$$

AV_f is the acid value of the PFAD feedstock and AV_p is the acid value of the PFAD biodiesel. Each esterification reaction was conducted three times, and each product was analysed in triplicate, and the data reported as a mean.

2.5 PFAD biodiesel analysis

The PFAD biodiesel produced under the optimised esterification conditions was qualitatively analysed using a gas chromatography-mass spectrometry instrument (GC-MS Agilent Technologies 6890N) that was equipped with a HP 5971A mass selective detector (MSD). A highly polar HP-5 MS capillary column (length: 30 m, ID: 0.25 mm and film thickness: 0.25 μm) was used for the separation of the FAME's components. Helium was used as a carrier gas at a flow rate of 1.5 ml min^{-1}. The liquid product was diluted with GC grade *n*-hexane (98.0% purity). About 1.5 μL of the diluted sample was injected into the port using the splitless injection mode. The temperature program was set from 70 to 280 °C with a heating rate of 4 °C min^{-1}. Both the injector port and detector temperatures were set at 280 °C. The mass spectroscopy detector employed 70 eV of ionisation energy, a scanning range within 50–300 amu and a 1 s^{-1} scanning rate. This experiment was repeated three times and the value variation was calculated. The database from the Library of National Institute of Standards and Technology (NIST) was used to identify all peaks detected in the GC chromatogram, which represents the existence of fatty acids. Next, the chemical functional groups present in the PFAD feedstock, PFAD biodiesel and B5 diesel were also compared using Fourier-transform infrared spectroscopy (FT-IR; Perkin Elmer (PC) Spectrum 100 FTIR). The resolution was 4 cm^{-1} in the IR range of 400–4000 cm^{-1}, and the attenuated total reflection (ATR) sampling method was used. The yield of fatty acid methyl ester was calculated using eqn (3):[24]

$$\text{FAME yield } (\%) = \frac{\text{FAME content}}{\mathrm{FFA_f}} \times 100 \quad (3)$$

FAME content is the methyl ester of PFAD biodiesel, while FFA_f is the FFA of the PFAD feedstock.

2.6 Catalyst reusability and sulfur leaching analysis

A reusability test was carried out to study the deactivation and recyclability of the catalyst. It was conducted under the optimised esterification conditions without any reactivation steps.

The spent catalyst was recovered, and washed with 1 ml of *n*-hexane, followed by 1 ml of methanol and acetone, respectively. The washed catalyst was then dried at 100 °C for 8 h, before proceeding to the next cycle. Note that the reaction cycle was stopped when the FFA conversion approached the steady state value of 50%. Solvent washing is essential to remove the non-polar and polar compounds that were attached to the catalyst surface. The spent catalyst collected in the last cycle was characterised to investigate the weight, structural, morphological and composition changes. The sulfur leaching from the catalyst into the biodiesel was also determined using a CHNS elemental analyser (Loco, USA).

3. Results and discussion

The PFAD feedstock had a moisture content of 0.1 wt%, a saponification value of 204.6 mg KOH per g and an average molecular weight of 274.2 g mol^{-1}. It also had an acid value of 190.2 mg KOH per g with 95.5% FFA content. These outcomes are still within an acceptable range as proposed by the MPOB (Malaysian Palm Oil Board). It is well-known that higher FFA content required superacid catalyst, either homogeneous or heterogeneous, is required to drive the esterification forward and produce biodiesel. In this study, various SnO_2 based catalysts were screened as solid acid catalysts for the esterification of PFAD feedstock. Among them, the sulfonated SnO_2-spc was found to be the most active catalyst and was further studied for the optimisation of the esterification reaction using the OVAT technique. Under the optimised conditions, the catalyst was also tested for reusability and sulfur leaching. The sulfonated SnO_2-spc catalyst was synthesised *via* the SPC method; with the aim of it being a facile approach to obtain the nanocatalysts. It involved dissolving the metal salt ($SnCl_2 \cdot 2H_2O$) and oxidising agent ($C_6H_8O_7 \cdot H_2O$) in a minimal amount of deionised water, leading to a green synthesis method as no organic solvent was used. The mixture was heated up to 350 °C, which is an auto-combustion temperature for citric acid. After that, the mixture started to bubble, thickening, smouldering and releasing brown fumes. A mild combustion phenomenon was observed and a blackish-grey dried powder was formed. Interestingly, the overall synthesis process was completed in less than 15 min. The SPC method was not only a green technique but also resulted in reduced reaction time. Subsequently, the resultant product was calcined at 600 °C for 6 h to give pure SnO_2 nanoparticles that were treated using chlorosulfonic acid. Fig. 1 portrays a schematic diagram of the SPC method, sulfonation treatment and esterification reaction.

3.1 Characterisation of the catalysts

Fig. 2 shows the thermal decomposition of the precursor obtained using the SPC method. A major weight loss of about 50% can be seen from 30 °C up to 400 °C. This was accompanied by a broad exothermic peak with its maximum temperature at 390 °C, implying precursor decomposition. Two small endothermic peaks (~80 °C and ~240 °C) also appeared in the DSC curve that were attributed to the removal of moisture and organic traces from the precursor as proposed previously.[25] The TGA curve showed no significant weight loss after 400 °C. Therefore, the formed precursor was calcined at 600 °C to give pure SnO_2-spc, as confirmed using XRD analysis.

As mentioned, four SnO_2 based catalysts were investigated, and the colour of each powder is shown in Fig. 3(a). The synthesised catalysts look darker than the commercialised catalysts. The colour difference suggests a variation in the catalyst properties. Fig. 3(b) shows their X-ray diffraction patterns. All of the catalysts exhibited XRD peaks at 2θ = 26.6°, 33.9°, 37.9°, 39.0°, 51.7°, 54.7°, 57.8°, 61.9°, 64.7°, 65.9°, 71.2° and 78.7°, which were indexed as (110), (101), (200), (111), (211), (220), (002), (310), (112), (301), (202) and (321) crystal planes. According to the International Centre for Diffraction Data through ICDD 01-002-1340, this XRD pattern belongs to the tetragonal crystal structure of crystalline SnO_2. Also, the formed catalysts were pure with no impurity peaks detected by XRD, except that the peak intensity was reduced after the sulfonation treatment using chlorosulfonic acid. As reported by Ahmed and co-workers,[26] the intensity reduction of the XRD peaks may be due to the attachment of acidic ions (HSO_3^-) on the catalyst surface affecting the textural and acidity properties. The presence of sulfur (S) in the sulfonated SnO_2 catalysts was detected by both EDX and CHNS analyses, as tabulated in Table 1. It has been found that the amount of S species was higher for the sulfonated SnO_2-spc as compared to the sulfonated SnO_2-com.

Table 1 also shows the crystallite size, specific surface area (S_{BET}), total pore volume and average pore diameter of the catalysts. The crystallite size was estimated using the Debye–Scherrer equation at the most intense peak of the (110) crystal plane. It showed that the SnO_2-spc was smaller in crystallite size than the SnO_2-com, causing the SnO_2-spc to have a larger surface area for the attachment of HSO_3^- ions. For the non-sulfonated catalysts, the S_{BET} values for SnO_2-com and SnO_2-spc were 6.8 $m^2\ g^{-1}$ and 7.5 $m^2\ g^{-1}$. As expected, these values decreased after the sulfonation treatment. About a 73.3% decrease in S_{BET} was observed for the sulfonated SnO_2-spc, while it was only 1.5% for the sulfonated SnO_2-com. This indicated that the sulfonated SnO_2-spc should be a more acidic catalyst than the sulfonated SnO_2-com. A similar trend was also observed for the total pore volume and average pore diameter for the catalysts, proposing that HSO_3^- ions have a greater tendency to be located inside the pores and/or block the pores as reported elsewhere.[27] As shown in Table 1, the pore distribution was within the mesoporous range (2 nm < d < 50 nm). However, this mesoporosity did not occur as proven by their N_2 adsorption–desorption isotherms (Type II) in Fig. 3(c), which reflect the macroporous character. There are only voids between the particles.

The FESEM images of all the catalysts are illustrated in Fig. 4(a). A significant difference in terms of morphology and particle size can be seen among the non-sulfonated and sulfonated SnO_2 catalysts. As shown in Fig. 4(a)(i), the SnO_2-com was composed of a mixture of particles with various shapes and sizes. Meanwhile, the SnO_2-spc (Fig. 4(a)(ii)) displayed smaller particles below than 100 nm with a homogenous spherical shape. After sulfonation (Fig. 4(a)(iii) and (iv)), the

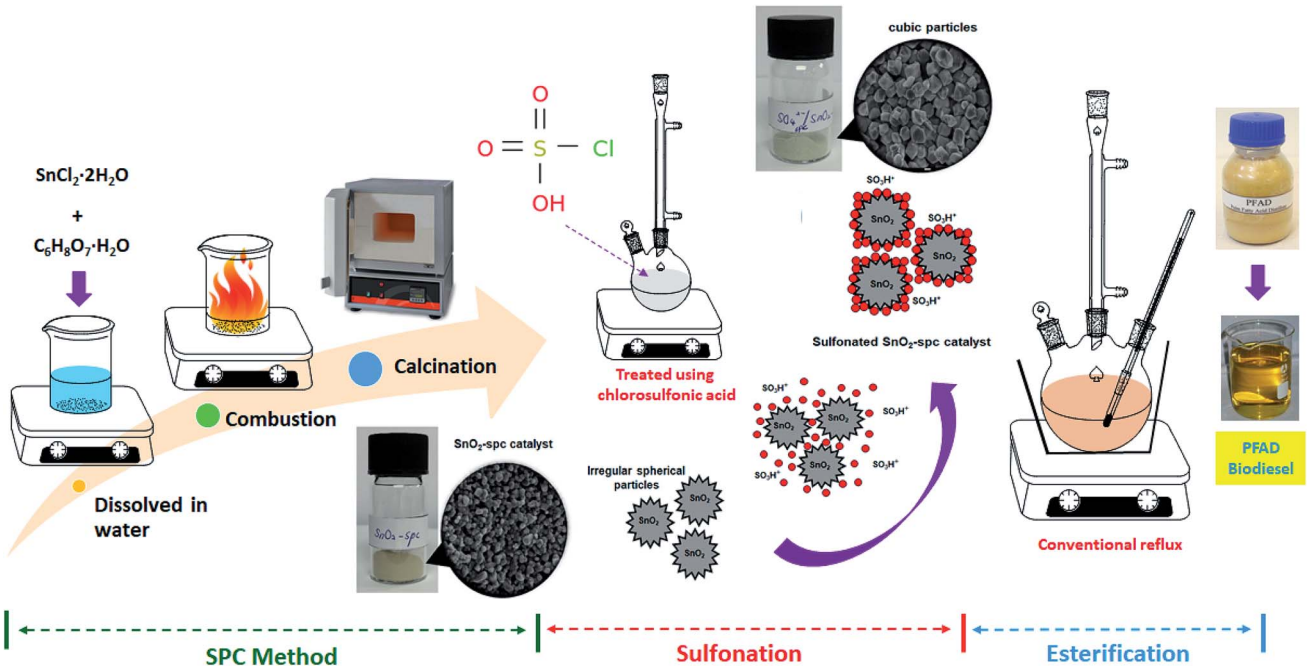

Fig. 1 Schematic diagram of the catalyst synthesis and esterification of the PFAD feedstock.

particle sizes for both catalysts increased with the sulfonated SnO_2-spc growing considerably due to more HSO_3^- ions attached to the SnO_2 surface. A similar trend was also reported previously.[28] This finding agreed very well with the S_{BET} values in Table 1, in which the smallest particles were responsible for the largest S_{BET} value, and *vice versa*.

The acidity properties of the SnO_2 based catalysts are shown in Fig. 4(b) and tabulated in Table 1. All of the catalysts, except for SnO_2-com, exhibited super acidic properties (T_{max} > 700 °C). Both the acid strength and acid density follow the trend of SnO_2-com < SnO_2-spc < sulfonated SnO_2-com < sulfonated SnO_2-spc. Note that the sulfonated SnO_2 catalysts displayed a remarkable increase in total acid density as compared to the non-sulfonated SnO_2 catalysts, suggesting that the existence of HSO_3^- ions enhanced their acidity properties.[29] Moreover, the non-sulfonated and sulfonated SnO_2-spc catalysts showed the formation of medium acidic sites with a maximum desorption peak at T_{max} of 462 °C and 362 °C, respectively. These peaks correspond to Lewis acid sites on the SnO_2 catalysts.[30] A Lewis acid is important for the electron-withdrawing effect of HSO_3^- groups that modify the acidity of the SnO_2 catalysts.[10] Since the sulfonated SnO_2-spc catalyst had the largest formation of super acidic sites as presented in Table 1, it is expected that this catalyst will be effective for the esterification reaction.

3.2 Catalytic screening of the catalysts

The preliminary catalytic screening for the studied SnO_2 catalysts in the esterification of PFAD feedstock was performed under identical conditions (methanol-to-PFAD molar ratio of 9 : 1, catalyst loading of 3 wt%, reaction temperature of 100 °C and reaction time of 3 h) to identify the most effective catalyst. Herein, their catalytic activities were compared based on the FFA conversion, as shown in Fig. 4(c). For the non-sulfonated catalyst, both SnO_2-com and SnO_2-spc exhibited mild esterification activities giving FFA conversions of 10.8% and 62.6%, respectively. This confirmed that the SnO_2 can be categorised as a superacid solid catalyst.[31] Based on Table 1, the SnO_2-spc possessed a relatively similar acidity strength to the sulfonated SnO_2-com with a different acid site density. This showed that the synthesis method (SPC technique) influenced its acid properties. Although the acid density of SnO_2-spc was lower than that of the sulfonated SnO_2-com, its homogenised smaller particle sizes (refer Fig. 4(a)(ii)) may reduce the diffusion limitation between the PFAD–methanol–SnO_2 phases, thus resulting in effective collisions and producing higher esterification activities. The sulfonated catalysts demonstrated higher FFA conversion up to 68.7% for the sulfonated SnO_2-com and 86.9% for the sulfonated SnO_2-spc. Among them, the sulfonated SnO_2-spc contained the

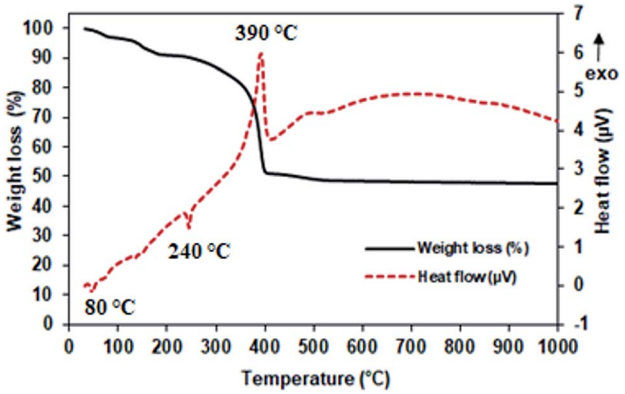

Fig. 2 TGA/DSC curves of the obtained precursor.

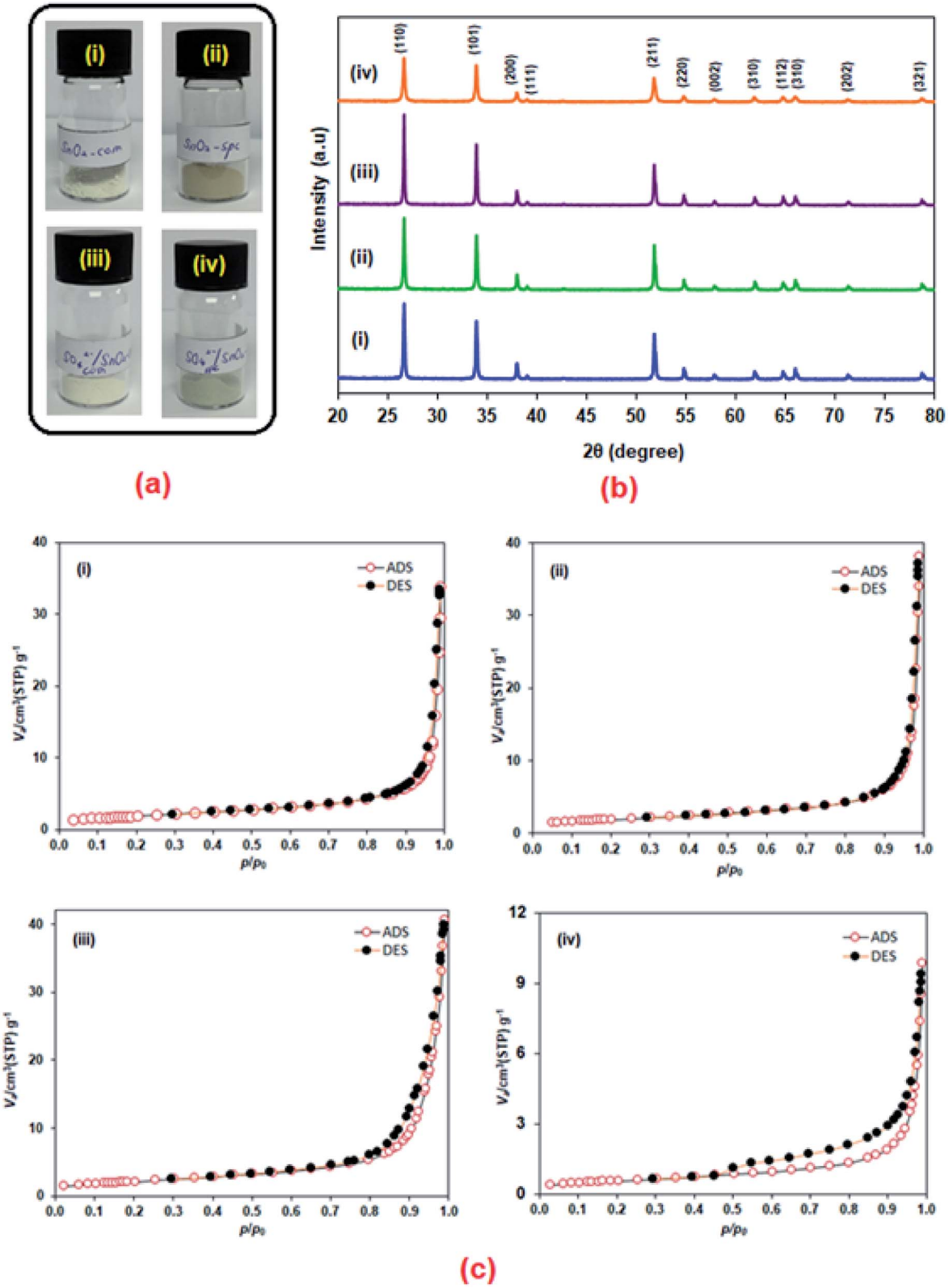

Fig. 3 (a) The colour of the catalyst powders, (b) XRD patterns and (c) N_2 adsorption–desorption isotherms of the (i) SnO_2-com, (ii) SnO_2-spc, (iii) sulfonated SnO_2-com and (iv) sulfonated SnO_2-spc catalysts.

highest total acid density of 5303.6 μmol g^{-1}. The greater density of acidic sites and superior acid strength play key roles in enhancing the esterification of the PFAD feedstock. A positive correlation between acidity and esterification performance has also been highlighted in the literature when high FFA of PFAD was used as the feedstock for biodiesel production.[24,32]

Table 1 Textural and acidity properties of the non-sulfonated and sulfonated SnO_2 catalysts

Catalyst	Crystallite size[a] (nm)	Sulfur content EDX[b] (wt%)	Sulfur content CHNS[c] (ppm)	Specific surface area[d] ($m^2\ g^{-1}$)	Total pore volume[d] ($\times 10^{-4}\ cm^3\ g^{-1}$)	Average pore diameter[d] (nm)	NH_3 desorption temperature[e] (°C)	Amount of NH_3 desorbed[e] ($\mu mol\ g^{-1}$)
SnO_2-com	77.5	ND	ND	6.8	5.6	33.2	ND	ND
Sulfonated SnO_2-com	77.7	0.2	474.1	6.7	5.1	30.0	341 796	125.2 1775.5
SnO_2-spc	16.9	ND	ND	7.5	6.1	32.6	426 773	49.5 72.6
Sulfonated SnO_2-spc	90.4	0.5	2128.9	2.0	1.5	28.5	362 825	317.6 4986.0

[a] Estimated using Debye–Scherrer's formula. [b] Determined by FESEM-EDX. [c] Determined by CHNS. [d] Calculated by BET. [e] Measured by TPD-NH_3. ND – not detected.

3.3 Optimisation of PFAD esterification

The esterification conditions using the sulfonated SnO_2-spc as the active catalyst were optimised considering various variables. Firstly, a series of reactions were carried out at different molar ratios of methanol-to-PFAD (3 : 1, 6 : 1, 9 : 1, 12 : 1, 15 : 1). In contrast, other variables such as reaction temperature (100 °C), catalyst loading (3 wt%) and reaction time (3 h) were kept constant to maximise the FFA conversion. Stoichiometrically, the methanol-to-PFAD molar ratio is only 1 : 1 to produce one mole of FAME and one mole of water. However, the esterification reaction is reversible; thus, a higher molar ratio can minimise the reverse reaction and boost the product yields. The obtained results are shown in Fig. 5(a). The FFA conversion markedly increased on increasing the methanol-to-PFAD molar ratio with the value at 9 : 1 recording the highest FFA conversion of 86.9%. This showed that at this molar ratio, the methanol and PFAD were miscible, which also reduced the mass transfer limitation in methanol–PFAD–catalyst phases. However, further increasing the molar ratio up to 15 : 1, the FFA conversions slightly dropped. This phenomenon may be explained by the following factors: (1) the excess methanol flooding the active catalyst sites and hindering the protonation of FFA.[33] (2) The polar hydroxyl group of the excess methanol emulsifying the product and forming gels that were difficult to separate from the methyl ester.[34] The excess methanol may also produce a large amount of water as a side product that increased the cost of biodiesel production. Therefore, the methanol-to-PFAD molar ratio of 9 : 1 was selected for further studies.

Secondly, Fig. 5(b) shows the effect of catalyst loading (1–5 wt%) on the FFA conversion at a methanol-to-PFAD molar ratio of 9 : 1, reaction temperature of 100 °C and reaction time of 3 h. The presence of a catalyst with adequate active sites is crucial to surpass the activation energy and to enhance the esterification. The catalyst is not consumed during the reaction, and thus can be recovered and recycled for the next reaction. As expected, the lowest catalyst loading of 1 wt% gave the lowest FFA conversion of 68.3%. This conversion percentage continuously increased up to 98.9% at a catalyst loading of 4 wt%, which provided greater acid active sites for the esterification and accelerating the reaction rate. According to Fadhil and other researchers,[15] higher catalyst loading enriches it with hydrophilic functional groups such as –COOH and –OH, including sulfonic groups, catalysing the esterification between the polar FFA and methanol molecules. However, no improvement can be observed at 5 wt%. An excessive amount of catalyst increased the viscosity of the reaction mixture, which was detrimental to the mass transfer and inhibited the protonation of FFA.[35] The catalyst loading of 4 wt% was chosen as the optimum amount.

Thirdly, the influence of reaction temperature on the FFA conversion was studied within the range of 80 to 160 °C with a methanol-to-PFAD molar ratio of 9 : 1, catalyst loading of 4 wt% and reaction time of 3 h throughout all the experiments. Activation energy is required to protonate FFA since the esterification reaction is exothermic.[36] Generally, as the temperature increases, all of the reactant molecules gain more kinetic energy, which eventually accelerates the mass transfer rate between the oil–methanol–catalyst phases and results in the enhancement of esterification of the PFAD feedstock.[31] As shown in Fig. 5(c), the reaction temperature at 100 °C caused the highest FFA conversion of 98.9%. However, it was also observed that the FFA conversion seemed to be insignificant, even when further increasing the reaction temperature as reported in a previous study where too high a temperature could affect the physical appearance of the biodiesel, such as the darkness of the biodiesel.[36] Therefore, 100 °C was chosen as the optimum reaction temperature.

Last but not least, ample contact time was also vital for the optimum FFA conversion during the esterification of the PFAD feedstock. The reaction time was varied, ranging from 1 h to 5 h with a 9 : 1 methanol-to-PFAD molar ratio, 4 wt% of catalyst loading and 100 °C reaction temperature. The FFA conversion at different reaction times is shown in Fig. 5(d). Note that the FFA conversion momentously increased from 89.6% to 98.9% when the reaction time was prolonged from 1 h to 3 h. Extending the reaction time to 5 h was unnecessary, since the FFA conversion only increased by 0.2%. Therefore, a reaction time of 3 h was chosen with a methanol-to-PFAD molar ratio of 9 : 1, a catalyst loading of 4 wt% and

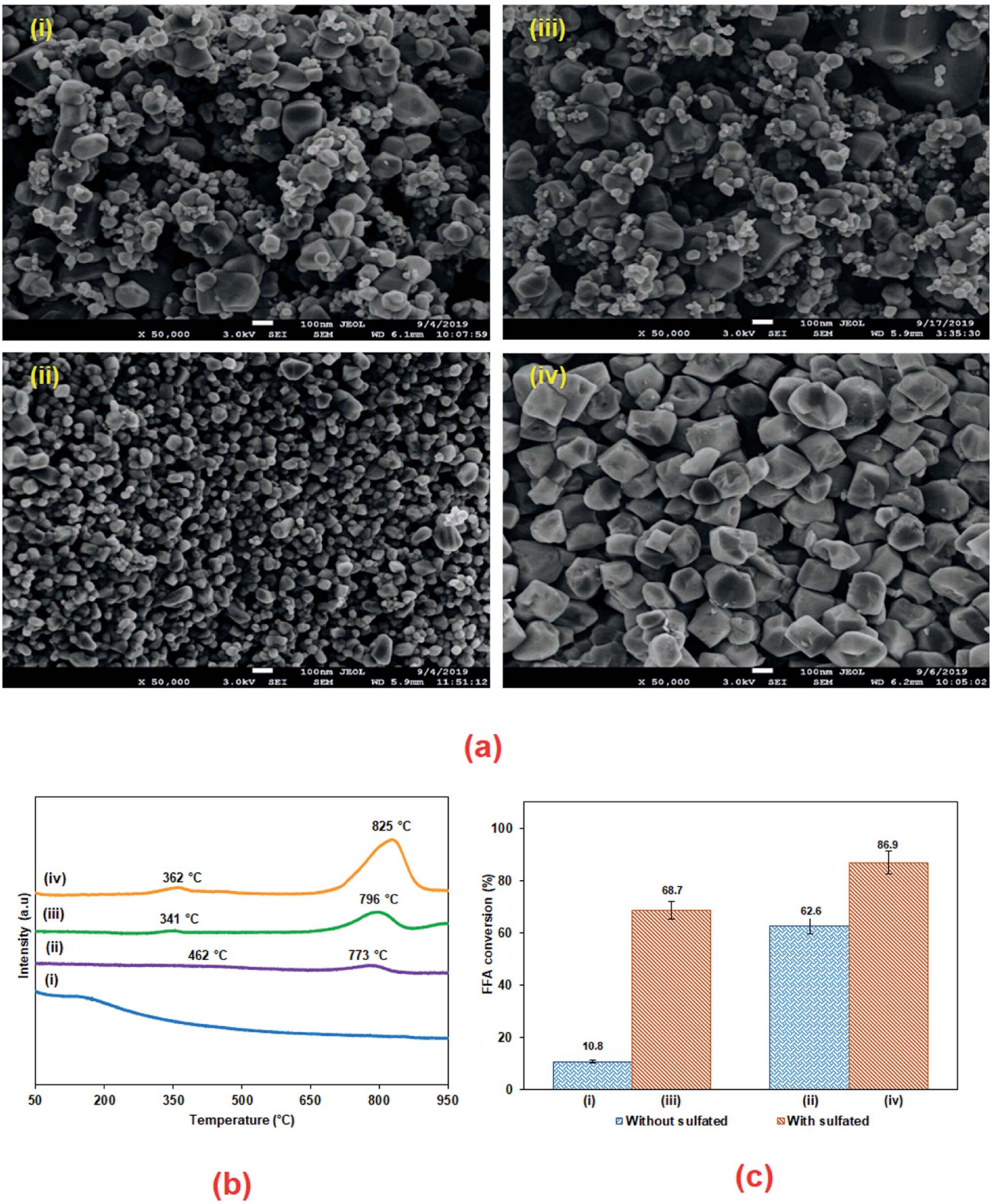

Fig. 4 (a) FESEM images, (b) TPD-NH_3 profiles and (c) preliminary screening of the catalytic performances of (i) SnO_2-com, (ii) SnO_2-spc, (iii) sulfonated SnO_2-com and (iv) sulfonated SnO_2-spc catalysts. The esterification was performed at a methanol-to-PFAD molar ratio of 9 : 1, catalyst loading of 3 wt%, temperature of 100 °C, and reaction time of 3 h.

a reaction temperature of 100 °C as the optimum esterification conditions, effectively catalysed by the sulfonated SnO_2-spc catalyst resulting in a maximum FFA conversion of 98.9%. Optimising the esterification conditions is an important economic consideration to make the production of biodiesel feasible.

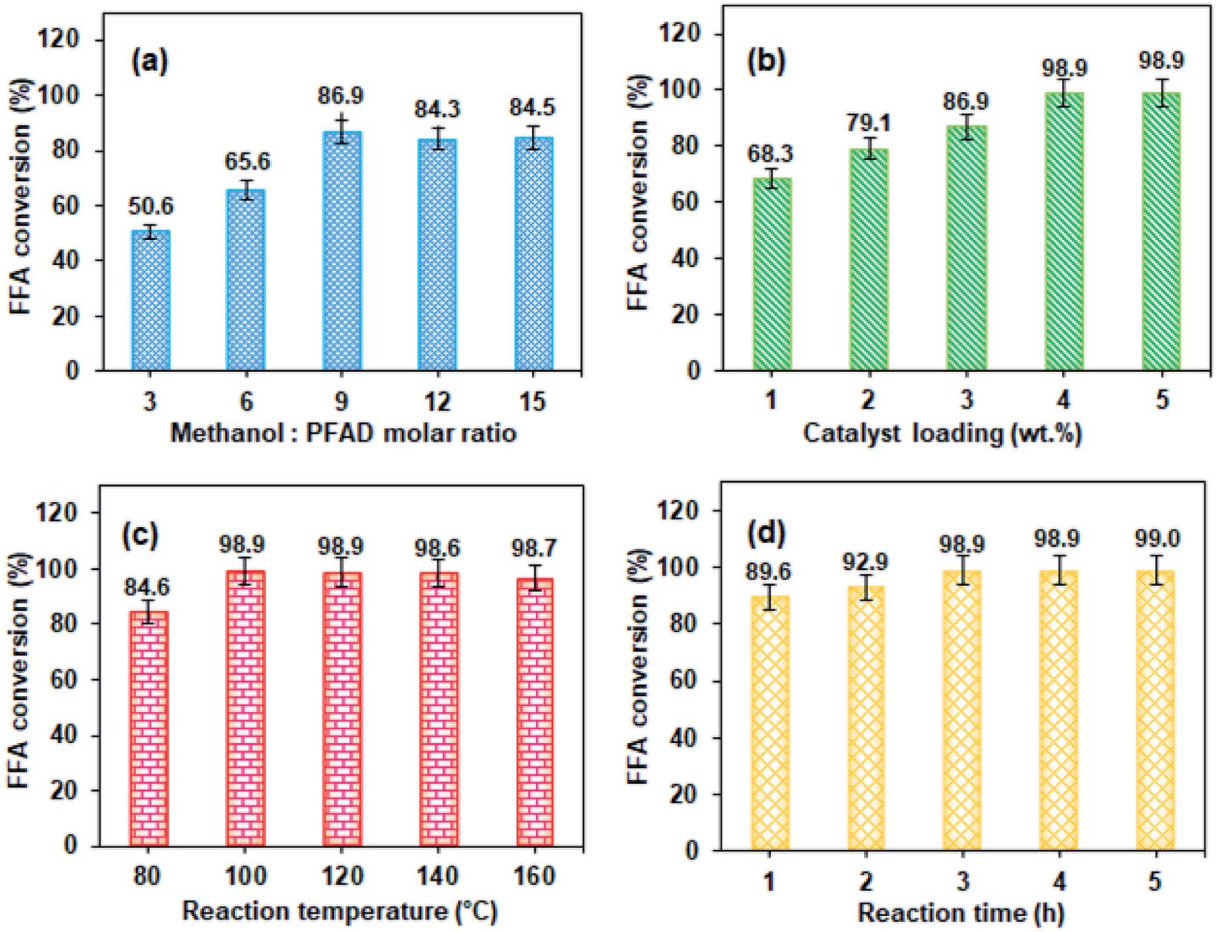

Fig. 5 FFA conversion for esterification of the PFAD feedstock over the sulfonated SnO_2-spc catalyst at different variables: (a) the effect of methanol-to-PFAD molar ratio (temperature: 100 °C, catalyst loading: 3 wt%, and reaction time: 3 h). (b) The effect of catalyst loading (methanol-to-PFAD: 9 : 1, temperature: 100 °C, and reaction time: 3 h). (c) The effect of reaction temperature (methanol-to-PFAD: 9 : 1, catalyst loading: 4 wt% and reaction time: 3 h). (d) The effect of reaction time (methanol-to-PFAD: 9 : 1, catalyst loading: 4 wt% and reaction temperature: 100 °C).

Fig. 6 proposes the mechanism for esterification of FFA of the PFAD feedstock with methanol in the presence of a sulfonated SnO_2 catalyst. It is a straightforward mechanism. As reported in the literature,[37,38] a solid acid catalyst with a greater number of protons will attack the oxygen atom of the carbonyl (C═O) of the FFA and form electrophilic intermediates. This means that the $-SO_3H$ groups that attached to the SnO_2 catalyst acted as a proton donor and Lewis acid, and are known as active sites for protonation. In other words, the intermediate formation occurred through the Lewis acid–FFA interactions. This intermediate allowed nucleophilic attack by the added methanol. The lone pair belonging to methanol will be combined with the protonated intermediate and release water as a by-product; thus, the protonated ester was formed. Sufficient methanol is required to shift the esterification forward and avoid the reverse reaction. Finally, the proton of the protonated ester was transferred back to the deprotonated catalyst and produced FAME.

3.4 Properties of PFAD biodiesel

Both the PFAD feedstock and PFAD biodiesel were analysed using GC-MS. Fig. 7(a) displays the GC-MS chromatogram for the PFAD biodiesel after it was produced under the optimised esterification conditions. From the GC-MS analysis, the PFAD feedstock contained predominantly 50.5% of palmitic acid (C16:0) and 43.6% of oleic acid (C18:1). After the esterification, these FFAs were converted to methyl palmitate (48.6%) and methyl oleate (39.6%) as the main composition of the PFAD biodiesel. In total, about 93.8% FAME was formed. This finding also agreed with the IR-ATR results, in which the PFAD biodiesel and the B5 diesel showed different absorption bands as compared to the PFAD feedstock (Fig. 7(b)). All the samples exhibited notable absorption bands at 2860 and 2920 cm^{-1} belonging to the asymmetric stretching vibration of the C–H group. C–H bending modes were also observed at 1377, 1400 and 1462 cm^{-1}.[39] The PFAD feedstock showed an absorption band at 1700 cm^{-1} for its –COOH group. This absorption band was shifted to 1744 cm^{-1} for the PFAD biodiesel and B5 diesel, which was attributed to the C═O stretching vibration of the methyl esters. Importantly, another absorption band at 1436 cm^{-1} also appeared for the PFAD biodiesel, indicating the formation of an $-OCH_3$ group. This revealed that the esterification of the PFAD feedstock to FAME could be achieved using the sulfonated SnO_2-spc catalyst. Both biofuels also have absorption bands within the range of 1000–

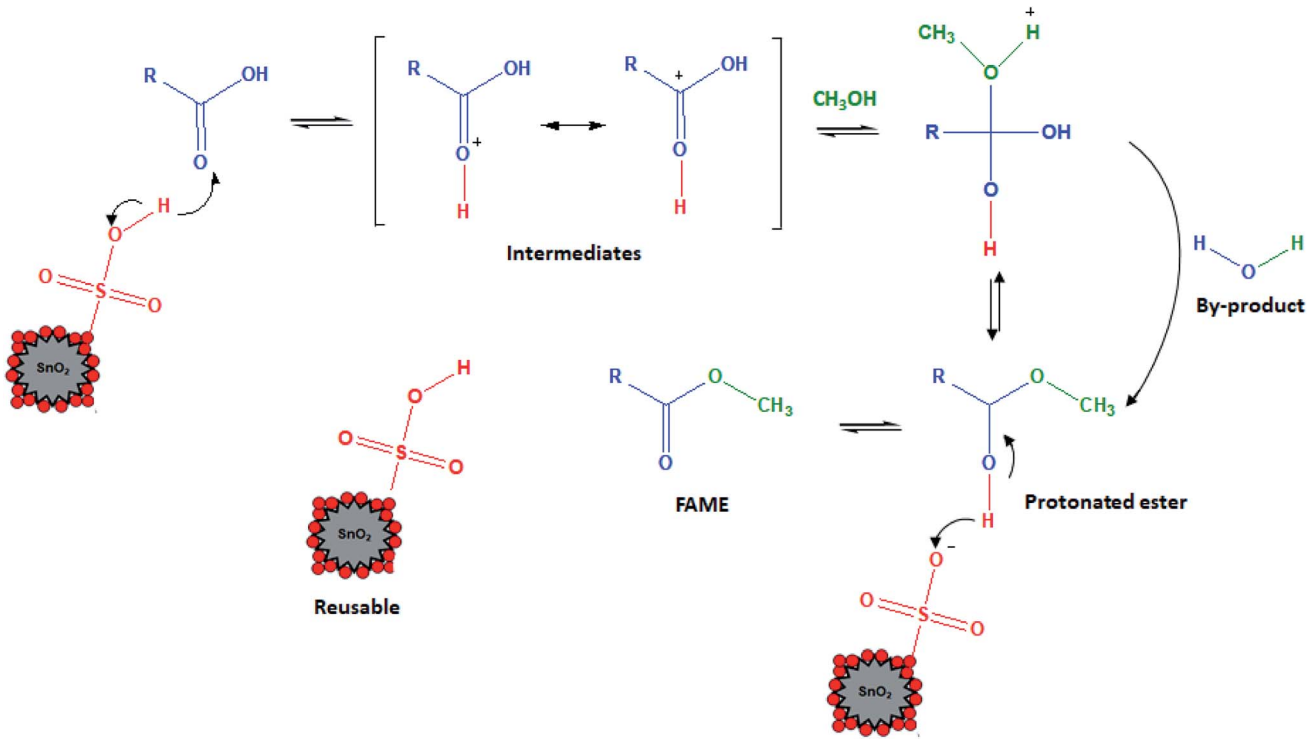

Fig. 6 Proposed mechanism for the esterification of PFAD into FAME over the sulfonated SnO_2-spc catalyst.

1300 cm^{-1}, which can be assigned as the C–O stretching vibration of the long-chain fatty acids.[40] Note that the existence of a high level of oxygenated species in the PFAD biodiesel resulted in a more intense peak for C=O groups (1744 cm^{-1}) as compared to the B5 diesel. The less intense C=O peak in the B5 diesel was due to the high blending ratio between diesel (95%) and biodiesel (5%). Even though a high level of oxygenated species (high oxygen content) is responsible for the increase of NO emissions, parenthetically, the presence of oxygenated species in the PFAD biodiesel may also improve the combustion efficiency of the fuel, which helps in reducing the hydrocarbon (HC) and carbon monoxide (CO) emissions as well as minimising the noise pollution.[41] Thus, the PFAD biodiesel is still superior to B5 diesel in terms of reducing the main greenhouse gases (GHG).

3.5 Reusability and leaching analysis of the sulfonated SnO_2-spc catalyst

A reusability test for the sulfonated SnO_2-spc catalyst was conducted under the optimised esterification conditions

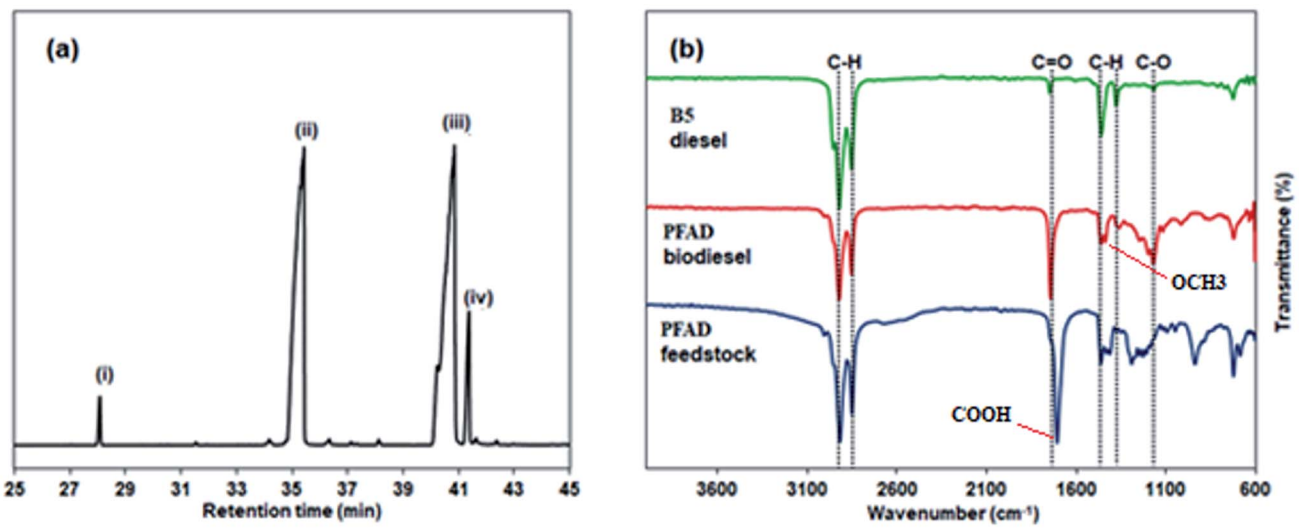

Fig. 7 (a) GC-MS chromatogram of PFAD biodiesel: (i) methyl myristate, (ii) methyl palmitate, (iii) methyl oleate and (iv) methyl linoleate. (b) IR-ATR spectra for the PFAD feedstock, PFAD biodiesel and B5 diesel.

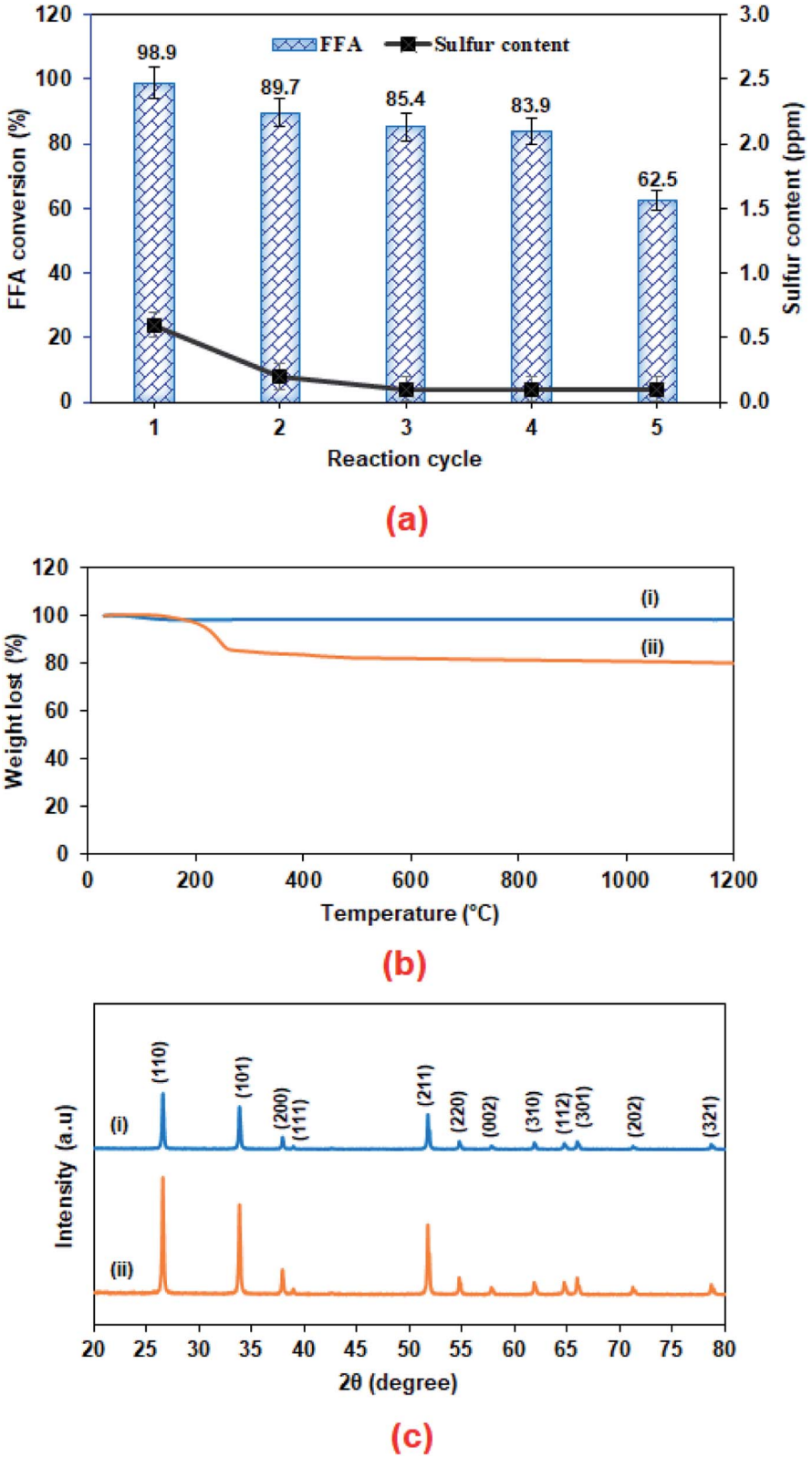

Fig. 8 (a) Reusability of the sulfonated SnO_2-spc catalyst and the amount of leached-sulfur estimated by CHNS elemental analysis for 5 cycles, and (b) TGA curves and (c) XRD patterns of the (i) fresh and (ii) spent sulfonated SnO_2-spc catalysts after 5 consecutive runs.

(methanol-to-PFAD molar ratio of 9 : 1, catalyst loading of 4 wt%, reaction temperature of 100 °C and reaction time of 3 h). After each cycle, the spent catalyst was recovered and washed using *n*-hexane followed by methanol and acetone to remove the adsorbed non-polar and polar compounds from the surface of the spent catalyst.[16] The results in Fig. 8(a) show that the

Table 2 FESEM-EDX mapping for the fresh and spent sulfonated SnO_2-spc catalysts

Catalyst	Fresh catalyst	Spent catalyst
FESEM image	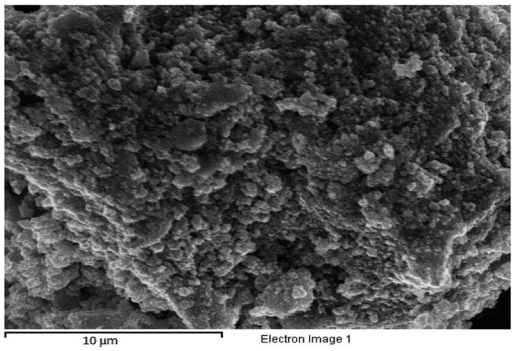	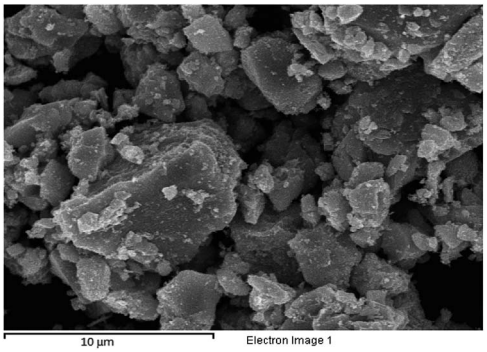
Sn (wt%)	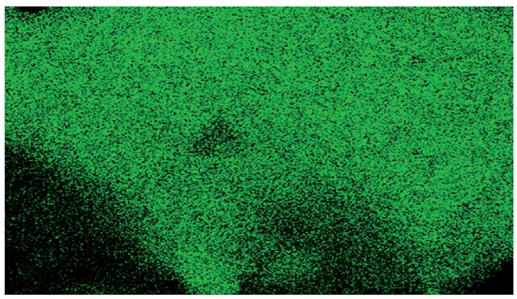 30.1	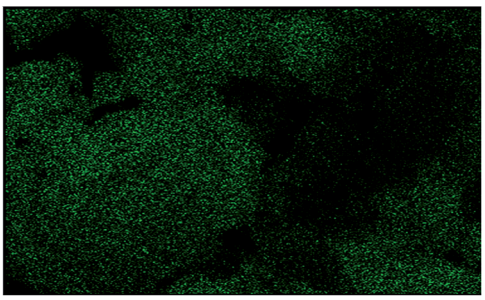 14.3
O (wt%)	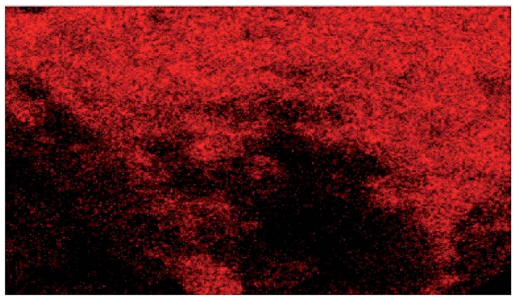 14.3	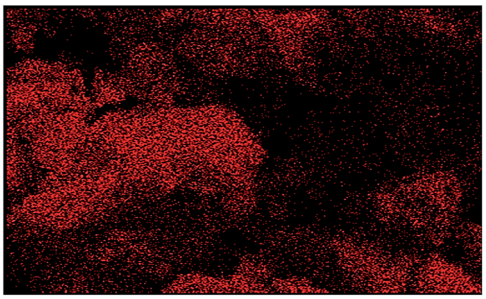 85.6
S (wt%)	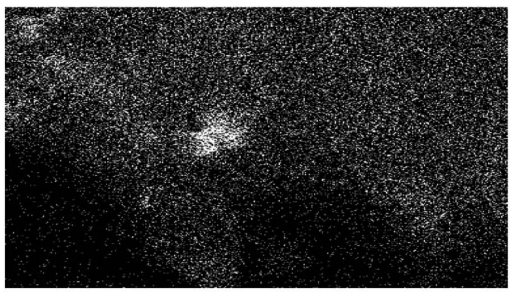 0.5	 0.1

esterification reaction maintained >80% FFA conversion after four consecutive runs. Further reaction resulted in an FFA conversion of about 63%. The change in properties between the fresh and spent sulfonated SnO_2-spc catalysts were studied *via* TGA, XRD, TPD-NH_3 and FESEM-EDX mapping. From the TGA results (Fig. 8(b)), the spent catalyst showed a weight loss of 20% starting at 250 °C, indicating the presence of carbon adsorbed on the catalyst surface. However, from the XRD patterns (Fig. 8(c)), the oxide phase of Sn for both the fresh and spent catalysts remains unchanged, except that the crystallinity

of the spent catalyst was found to be increased after five runs, due to multiple heat exposures during the esterification reaction. This means that the sulfonated SnO_2-spc catalyst was highly stable as proven by there being no phase changes before and after the reaction. Unfortunately, their acidity was reduced after a few reaction cycles, as given by the TPD-NH_3 outcomes. A remarkable reduction of acidic sites and acidic strength was observed for the spent sulfonated SnO_2-spc catalyst. After the reusability test, the medium acid region was lost entirely. Still, some of the strong acid sites were consumed during the PFAD esterification and formed a medium acidic site at 419 °C with 813.0 μmol g^{-1}. Several studies have reported that the acidic characters of the catalyst gradually reduced after multiple esterification cycles and thereby may result in a loss of catalytic activities.[42,43] These studies suggested that the loss of inherent acidic character of the catalyst was possibly associated with leaching of the S groups from the surface of the sulfonated SnO_2-spc. This shows that the S composition of the spent catalyst exhibited 80% reduction of S (refer to Table 3) as compared to the fresh catalyst. Considering this, a decrease in S species in the spent catalyst is expected to reduce the acid sites. Furthermore, the elemental analysis of fresh and spent sulfonated SnO_2-spc catalysts was also performed *via* the FESEM-EDX mapping technique. The surface morphology before and after the consecutive runs looks very different, which was ascribed to crystallite growth upon heat exposure. This did not change the crystal structure of the SnO_2 catalyst as proved by the XRD patterns in Fig. 8(c), meaning that the SnO_2 structure is highly stable even after been subjected to heating several times. The results confirmed that there was leaching of Sn and S after the esterification reaction, as stated in Table 2. The sulfur leached into the biodiesel was also quantified using CHNS analysis, and the findings are shown in Fig. 8(a). The leaching of Sn and S from the catalyst was possible after continuous heating and a prolonged reaction duration.[44] Even though the catalyst structure seemed to be stable after being reused in a few cycles, the reduction in acidity and the leaching of both Sn and S is still responsible for the sudden drop of the FFA conversion, especially from cycle 4 to cycle 5 with almost 20% difference. A greater acid density is required to esterify the highest FFA content of the PFAD feedstock into FAME. The catalyst deactivation can be suppressed by employing catalyst regeneration and reactivation steps.[45] Although the sulfur was leached out into the biodiesel, the concentration detected was lower than the maximum limit (25 ppm) in ASTM D6751-02.[46] Overall, these findings suggested that the reduction of the esterification activity in the spent sulfonated SnO_2-spc catalyst after four consecutive runs was due to the accumulation of carbon species, loss of acidic sites and leaching of S species.

3.6 Comparison of metal oxide catalyst-based esterification reactions

SnO_2 based catalysts have been recognised as a solid acid catalyst and used in many chemical reactions including the esterification of diverse feedstocks.[47] Previously, SO_4^{2-}/SnO_2 esterified levulinic acid,[48] SO_4^{2-}/SiO_2–SnO_2 esterified *Moringa oleifera* oil,[49] SO_4^{2-}/Co_2O_3–SnO_2 esterified crude palm oil,[13] and both CaO–SnO_2 and WO_3–SnO_2 esterified soybean oils[2,50] have been used as feedstocks with lower FFA contents than the PFAD feedstock. The esterification of PFAD into biodiesel is rather challenging due to its high FFA, which requires a superacid catalyst for maximum FFA conversion and high FAME yield. Table 3 presents the catalytic performances of various metal oxide catalysts for the esterification of the PFAD feedstock. Embong *et al.*[51] used SO_4^{2-}/TiO_2–SiO_2 and Soltani *et al.*[52] used HSO_3^-/CuO–ZnO as the solid acid catalysts, and the FFA conversions were 93.3% and 96.1%, respectively. Both catalysts are mixed metal oxides treated with a strong acid. More acidic metal oxides such as ZrO_2 were also studied for the

Table 3 Summary of recent studies on esterification of the PFAD feedstock using metal oxide catalysts

Catalyst (synthesis method for metal oxide)	Chemical activation	Esterification	Optimal reaction parameters				FFA conversion (%)	FAME yield (%)	Ref.
			MeOH : PFAD molar ratio	Catalyst loading (wt%)	Temp (°C)	Time (h)			
SO_4^{2-}/SnO_2 (precipitation)	H_2SO_4	Thermocouple reactor	5 : 1	2.5	70	7.5	—	77.0	48
SO_4^{2-}/SnO_2–SiO_2 (commercial)	H_2SO_4	Thermocouple reactor	19.5 : 1	3.0	150	2.5	—	95.0	49
SO_4^{2-}/TiO_2–SiO_2 (wet impregnation)	H_2SO_4	Conventional reflux	5.85 : 1	2.97	150	3.12	93.3	—	51
HSO_3^-/CuO–ZnO (hydrothermal)	$C_6H_6O_3S$	Autoclave reactor	9 : 1	1.5	100	1.5	96.1	—	52
MnO–NiO–SO_4^{2-}/ZrO_2 (wet impregnation)	HSO_3Cl	Conventional reflux	15 : 1	3	70	3	97.7	—	53
HSO_3^-/ZrO_2 (precipitation)	HSO_3Cl	Glass reactor	8 : 1	3.5	60	2.5	91.5	90.2	54
HSO_3^-/ZnO (hydrothermal)	H_2SO_4	Autoclave reactor	9 : 1	2	120	1.5	95.6	91.8	16
HSO_3^-/SnO_2 (SPC)	HSO_3Cl	Conventional reflux	9 : 1	4	100	3	98.9	93.8	This work

esterification of PFAD into FAME. Al-Jaberi *et al.*[53] esterified the PFAD feedstock using a $MnO–NiO–SO_4^{2-}/ZrO_2$ catalyst. The FFA conversion was 97.7%, which was slightly higher than that given by the first row transition metal oxide-based catalysts. However, the ZrO_2 was supported with double metal oxides (MnO–NiO) to amplify the acid properties and it was treated using a stronger acid such as chlorosulfonic acid. The utilisation of this catalyst for biodiesel production increased the total cost. Note that the catalyst was prepared *via* the conventional synthesis method, called wet impregnation, which was the main reason for the less impressive catalyst properties. More sophisticated synthesis methods like precipitation and hydrothermal methods have been explored by other researchers. The HSO_3^-/ZrO_2 and HSO_3^-/ZnO catalysts[16,54] both gave acceptable FFA conversions and FAME yields. This indicated that the synthesis method might affect the catalyst properties and catalytic performance. We reported the synthesis of the HSO_3^-/SnO_2 catalyst using the SPC method. Interestingly, it only used water as a solvent with a minimal amount, completed in a short reaction time and readily formed a dried powder before calcination. Furthermore, this synthesis method also resulted in a nano-sized metal oxide that anchored many acid ions and enhanced the acid properties, which induced the esterification reaction. The formed catalyst showed a high esterification performance of 98.9% FFA conversion and 93.8% FAME yield at a methanol-to-PFAD molar ratio of 9 : 1, catalyst loading of 4 wt%, reaction temperature of 100 °C and reaction time of 3 h. It is worth mentioning that the SPC method is a simple and green approach. The HSO_3^-/SnO_2 as a solid acid catalyst not only widened the catalyst choices, but was also cost-effective because the non-transition metal is cheaper than the d-block and f-block elements.

4. Conclusions

A superacid solid catalyst of SnO_2 was synthesised *via* the SPC method, followed by a chemical activation using chlorosulfonic acid. This synthesis method is a simple, green technique, and produced homogeneous nano-sized particles that covalently anchored many HSO_3^- ions, thus enhancing the catalyst acid strength, which are important criteria for the esterification of high FFA feedstocks such as PFAD. The highest FFA conversion of 98.9% with a 93.8% FAME yield was achieved at the optimised methanol-to-PFAD molar ratio of 9 : 1, catalyst loading of 4 wt%, reaction temperature of 100 °C and reaction time of 3 h. The sulfonated SnO_2-spc catalyst can be recycled in up to five consecutive runs with acceptable FFA conversion. It was also found that the synthesised sulfonated SnO_2 catalyst showed a remarkable catalytic performance compared to the commercial sulfonated SnO_2 catalyst. It was concluded that the selection of the synthesis method is crucial in designing an effective catalyst to reduce the cost of biodiesel production from low value, cheaper, abundant and non-edible PFAD feedstocks.

Conflicts of interest

There are no conflicts of interest to declare.

Acknowledgements

The authors would like to acknowledge the Ministry of Higher Education of Malaysia for the financial support under the Fundamental Research Grant Scheme (No. Grant: 600-IRMI/FRGS 5/3 (036/2019)).

References

1 A. E. Atabani, A. S. Silitonga, I. A. Badruddin, T. M. I. Mahlia, H. H. Masjuki and S. Mekhilef, *Renewable Sustainable Energy Rev.*, 2012, **16**, 2070–2093.
2 W. Xie and L. Zhao, *Energy Convers. Manage.*, 2013, **76**, 55–62.
3 N. Mansir, Y. H. Taufiq-Yap, U. Rashid and M. L. Ibrahim, *Energy Convers. Manage.*, 2017, **141**, 171–182.
4 T. A. Almeida, I. A. Rodrigues, T. S. Estrela, C. N. F. Nunes, L. L. Machado, K. V. Leao, I. C. L. Barros, F. A. C. Amorim and V. S. Braga, *Energy*, 2016, **97**, 528–533.
5 A. Talebian-Kiakalaieh, N. A. S. Amin and H. Mazaheri, *Appl. Energy*, 2013, **104**, 683–710.
6 N. Z. Abdul Kapor, G. P. Maniam, M. H. A. Rahim and M. M. Yusoff, *J. Cleaner Prod.*, 2017, **143**, 1–9.
7 Zero and Rainforest Foundation Norway, *Palm Fatty Acid Distillate (PFAD) in biofuels*.
8 J. I. Moreno, R. Jaimes, R. Gómez and M. E. Niño-Gómez, *Catal. Today*, 2011, **172**, 34–40.
9 P. Manjunathan and G. V. Shanbhag, *Application of tin oxide-based materials in catalysis*, Elsevier Inc., 2020.
10 R. Varala, V. Narayana, S. R. Kulakarni, M. Khan, A. Alwarthan and S. F. Adil, *Arabian J. Chem.*, 2016, **9**, 550–573.
11 M. A. Alves-Rosa, J. Z. Vasconcellos, L. H. Vieira, C. V. Santilli and S. H. Pulcinelli, *Colloids Surf., A*, 2019, **583**, 124012.
12 W. Xie, H. Wang and H. Li, *Ind. Eng. Chem. Res.*, 2012, 225–231.
13 K. Nuithitikul and W. Hasin, *Int. J. Chem. React. Eng.*, 2014, **12**, 1–12.
14 V. M. Mello, G. P. A. G. Pousa, M. S. C. Pereira, I. M. Dias and P. A. Z. Suarez, *Fuel Process. Technol.*, 2011, **92**, 53–57.
15 A. B. Fadhil, A. M. Aziz and M. H. Al-Tamer, *Energy Convers. Manage.*, 2016, **108**, 255–265.
16 S. Soltani, U. Rashid, S. I. Al-Resayes and I. A. Nehdi, *J. Cleaner Prod.*, 2017, **144**, 482–491.
17 Y. Zong, Y. Cao, D. Jia and P. Hu, *Sens. Actuators, B*, 2010, **145**, 84–88.
18 R. Al-Gaashani, S. Radiman, N. Tabet and A. R. Daud, *Mater. Sci. Eng., B*, 2012, **177**, 462–470.
19 L. Wu, J. C. Yu, L. Zhang, X. Wang and S. Li, *J. Solid State Chem.*, 2004, **177**, 3666–3674.
20 H. Xue, Z. Li, X. Wang and X. Fu, *Mater. Lett.*, 2007, **61**, 347–350.
21 J. Zapata, A. Nicollet, B. Julien, G. Lahiner, A. Esteve and C. Rossi, *Combust. Flame*, 2019, **205**, 389–396.
22 E. A. Levashov, A. S. Mukasyan, A. S. Rogachev and D. V. Shtansky, *Int. Mater. Rev.*, 2017, **62**, 203–239.

23 M. S. Mastuli, N. Kamarulzaman, M. F. Kasim, A. M. Mahat, Y. Matsumura and Y. H. Taufiq-Yap, *J. Supercrit. Fluids*, 2019, **154**, 104610.
24 S. N. A. Jenie, A. Kristiani, Sudiyarmanto, D. S. Khaerudini and K. Takeishi, *J. Environ. Chem. Eng.*, 2020, **8**, 103912.
25 R. S. Ningthoujam and S. K. Kulshreshtha, *Mater. Res. Bull.*, 2009, **44**, 57–62.
26 A. I. Ahmed, S. A. El-Hakam, A. S. Khder and W. S. Abo El-Yazeed, *J. Mol. Catal. A: Chem.*, 2013, **366**, 99–108.
27 Y. Chen, Y. Cao, Y. Suo, G. Zheng, X. Guan and X. Zheng, *J. Taiwan Inst. Chem. Eng.*, 2015, **51**, 186–192.
28 A. Laaksonen, M. Kulmala, T. Berndt, F. Stratmann, S. Mikkonen, A. Ruuskanen, K. E. J. Lehtinen, M. D. Maso, P. Aalto, I. Riipinen, R. Janson, F. Arnold, M. Hanke, J. Ucker, B. Umann, K. Sellegri, Y. Viisanen and A. S. Unit, *Atmos. Chem. Phys.*, 2008, **2**, 7255–7264.
29 O. Nur Syazwani, M. L. Ibrahim, Wahyudiono, H. Kanda, M. Goto and Y. H. Taufiq-Yap, *J. Supercrit. Fluids*, 2017, **124**, 1–9.
30 S. Soltani, U. Rashid, R. Yunus and Y. H. Taufiq-Yap, *Fuel*, 2016, **178**, 253–262.
31 M. K. Lam, K. T. Lee and A. R. Mohamed, *Appl. Catal., B*, 2009, **93**, 134–139.
32 S. K. Sangar, C. S. Lan, S. M. Razali, M. S. A. Farabi and Y. H. Taufiq-Yap, *Energy Convers. Manage.*, 2019, **196**, 1306–1315.
33 J. C. Juan, J. Zhang, Y. Jiang, W. Cao and M. A. Yarmo, *Catal. Lett.*, 2007, **117**, 153–158.
34 M. A. M. Ali, R. M. Yunus, C. K. Cheng and J. Gimbun, *RSC Adv.*, 2015, **5**, 76743–76751.
35 S. Ganesan, S. Nadarajah, X. Y. Chee, M. Khairuddean and G. B. Teh, *Renewable Energy*, 2020, **153**, 1406–1417.
36 S. K. Sangar, O. Nur Syazwani, M. S. A. Farabi, S. M. Razali, G. Shobhana, S. H. Teo and Y. H. Taufiq-Yap, *Renewable Energy*, 2019, **142**, 658–667.
37 N. A. Ibrahim, U. Rashid, T. S. Y. Choong and I. A. Nehdi, *RSC Adv.*, 2020, **10**, 6098–6108.
38 S. F. Ibrahim, N. Asikin-Mijan, M. L. Ibrahim, G. Abdulkareem-Alsultan, S. M. Izham and Y. H. Taufiq-Yap, *Energy Convers. Manage.*, 2020, **210**, 112698.
39 I. Istadi, D. D. Anggoro, L. Buchori, D. A. Rahmawati and D. Intaningrum, *Procedia Environ. Sci.*, 2015, **23**, 385–393.
40 M. L. Ibrahim, N. N. A. Nik Abdul Khalil, A. Islam, U. Rashid, S. F. Ibrahim, S. I. Sinar Mashuri and Y. H. Taufiq-Yap, *Energy Convers. Manage.*, 2020, **205**, 112445.
41 S. Ahmed, M. H. Hassan, M. A. Kalam, S. M. Ashrafur Rahman, M. J. Abedin and A. Shahir, *J. Cleaner Prod.*, 2014, **79**, 74–81.
42 Y. Zhang, W. Wong and K. Yung, *Appl. Energy*, 2014, **116**, 191–198.
43 M. Gohain, A. Devi and D. Deka, *Ind. Crops Prod.*, 2017, **109**, 8–18.
44 Y. L. Cheryl-Low, K. L. Theam and H. V. Lee, *Energy Convers. Manage.*, 2015, **106**, 932–940.
45 S. F. Ibrahim, N. Asikin-Mijan, M. L. Ibrahim, G. Abdulkareem-Alsultan, S. M. Izham and Y. H. Taufiq-Yap, *Energy Convers. Manage.*, 2020, **210**, 112698.
46 I. M. Lokman, U. Rashid, Z. Zainal, R. Yunus and Y. H. Taufiq-Yap, *J. Oleo Sci.*, 2014, **63**, 849–855.
47 R. Varala, V. Narayana, S. R. Kulakarni, M. Khan, A. Alwarthan and S. F. Adil, *Arabian J. Chem.*, 2016, **9**, 550–573.
48 M. Popova, P. Shestakova, H. Lazarova, M. Dimitrov, D. Kovacheva, A. Szegedi, G. Mali, V. Dasireddy, B. Likozar, N. Wilde and R. Gläser, *Appl. Catal., A*, 2018, **560**, 119–131.
49 G. Kafuku, M. K. Lam, J. Kansedo, K. T. Lee and M. Mbarawa, *Fuel Process. Technol.*, 2010, **91**, 1525–1529.
50 W. Xie and T. Wang, *Fuel Process. Technol.*, 2013, **109**, 150–155.
51 N. H. Embong, G. P. Maniam, M. H. Mohd, K. T. Lee and D. Huisingh, *J. Cleaner Prod.*, 2015, **116**, 244–248.
52 S. Soltani, U. Rashid, I. A. Nehdi and S. I. Al-Resayes, *Chem. Eng. Technol.*, 2017, **40**, 1–10.
53 S. H. H. Al-Jaberi, U. Rashid, F. A. J. Al-Doghachi, G. Abdulkareem-Alsultan and Y. H. Taufiq-Yap, *Energy Convers. Manage.*, 2017, **139**, 166–174.
54 A. R. Gupta, P. P. Chiplunkar, A. P. Pratap and V. K. Rathod, *Waste Biomass Valorization*, 2020, DOI: 10.1007/s12649-020-00949-y.